

Approximately Equivariant Quantum Neural Network for $p4m$ Group Symmetries in Images

Su Yeon Chang^{*†}, Michele Grossi^{*}, Bertrand Le Saux[‡] and Sofia Vallecora^{*}

^{*}*IT Department, European Organization for Nuclear Research (CERN), CH-1211 Geneva, Switzerland*

[†]*Laboratory of Theoretical Physics of Nanosystems (LTPN), Institute of Physics, École Polytechnique Fédérale de Lausanne, CH-1015 Lausanne, Switzerland*

[‡]*Φ-lab European Space Agency, IT-00044, Italy*

Email: su.yeon.chang@cern.ch

Abstract—Quantum Neural Networks (QNNs) are suggested as one of the quantum algorithms which can be efficiently simulated with a low depth on near-term quantum hardware in the presence of noises. However, their performance highly relies on choosing the most suitable architecture of Variational Quantum Algorithms (VQAs), and the problem-agnostic models often suffer issues regarding trainability and generalization power. As a solution, the most recent works explore Geometric Quantum Machine Learning (GQML) using QNNs equivariant with respect to the underlying symmetry of the dataset. GQML adds an inductive bias to the model by incorporating the prior knowledge on the given dataset and leads to enhancing the optimization performance while constraining the search space. This work proposes equivariant Quantum Convolutional Neural Networks (EquivQCNNs) for image classification under planar $p4m$ symmetry, including reflectional and 90° rotational symmetry. We present the results tested in different use cases, such as phase detection of the 2D Ising model and classification of the extended MNIST dataset, and compare them with those obtained with the non-equivariant model, proving that the equivariance fosters better generalization of the model.

Index Terms—Quantum Machine Learning, Geometric Quantum Machine Learning, Equivariance, Image classification, Image processing

I. INTRODUCTION

During the last few years, Quantum Machine Learning (QML) has witnessed remarkable progress from diverse research perspectives as a promising application for the practical use of quantum computers [1]–[3]. In particular, Quantum Neural Networks (QNNs) are suggested as the most general and fundamental formalism to solve a plethora of problems while the architecture is completely agnostic to the given problem. They are often expected to improve existing machine learning (ML) techniques in terms of training performance [2], [4], convergence rate [5], [6], and generalization power [7]–[9].

However, they often suffer from issues due to complex loss landscapes, which are often non-convex and lead to many poor local minima [10]–[12]. In an effort to solve these issues, the field of Geometric Quantum Machine Learning (GQML) [13]–[19] is currently emerging, inspired by the classical Geometric Deep Learning (GDL) [20]–[22].

The main idea of GQML is to add sharp inductive bias [23] into the training model by incorporating prior knowledge on

the dataset [18], [19]. In practice, GQML aims to construct a parameterized QNN, which is equivariant under the action of the symmetry group associated with the input dataset, so that the same action is applied to the output of the QNN. Previous studies have heavily explored GQML both in terms of theories and applications, showing that GQML helps mitigate the issues often encountered in QML [19]. However, most studies still focus on the permutation symmetric group, S_n [13], [15], [18], $\mathbb{Z}_2 \otimes \mathbb{Z}_2$ symmetry applied in small toy applications [14], or a single symmetry element in the case of image classification [24].

We extend the study on GQML in the context of image classification by taking into account the *planar wallpaper symmetry* group, $p4m$, which includes the reflection and the 90° rotation. The $p4m$ symmetry group is the most common symmetry group observed in image datasets, which are already treated in classical GDL via Group Equivariant Convolutional Networks (GCNN) [21], [25]. Although symmetry in images is considered to hinder neural network training in general, there exist applications where the symmetry has ponderable importance, such as Earth Observation [26]–[29], medical images [30], symmetry-related physics datasets [31], etc.

In this work, we introduce the *$p4m$ -Equivariant Quantum Convolutional Neural Network* (EquivQCNN) for image classification. The results clearly prove that the equivariant neural network has the advantage in terms of generalization power, in particular, while using only a small number of training samples. Moreover, we show that the presence of small noise in the EquivQCNN training helps to classify the symmetric images better. Our study ultimately paves the way for GQML to tackle realistic image classification tasks, improving training performance.

This paper is structured as follows. First of all, we will briefly summarize in Section II the theoretical backgrounds required to understand GQML. Then, in Section III, we introduce the architecture of *Equivariant Quantum Convolutional Neural Network* (EquivQCNN) for the *planar wallpaper symmetry* group $p4m$ in the context of image classification. Section IV present our first result for EquivQCNN applied on reflectional and rotational symmetric images and prove its generalization power compared to the non-equivariant architecture. We finally conclude in Section V and propose a future

research direction.

II. PRELIMINARIES

This section summarizes the theoretical background on group symmetry and equivariance required to construct a GQML architecture for supervised learning. Consider a classical data space \mathcal{X} and a label space \mathcal{Y} . Each data sample $\mathbf{x} \in \mathcal{X}$ is associated with a label $\ell \in \mathcal{Y}$ with the underlying function $f : \mathcal{X} \rightarrow \mathcal{Y}$. The supervised learning aims to find y_θ , which is as close as possible to the ground truth f with the trained parameters θ .

In the case of QML, we construct a quantum feature map $\psi : \mathcal{X} \rightarrow \mathcal{H}$, which embeds the classical data into a quantum state in the Hilbert space \mathcal{H} . The input quantum state $|\psi(\mathbf{x})\rangle \in \mathcal{H}$ is then transformed via QNN, taking the most general form of a Variational Quantum Circuits (VQCs) $\mathcal{U}(\theta)$ which is parameterized by the rotation angles θ . The final prediction of the QNN for the input feature \mathbf{x} is given as an expectation value of the observable O :

$$y_\theta(\mathbf{x}) = \langle \psi(\mathbf{x}) | \mathcal{U}^\dagger(\theta) O \mathcal{U}(\theta) | \psi(\mathbf{x}) \rangle. \quad (1)$$

In general, QNN architecture is completely agnostic to the underlying symmetry of \mathcal{X} . GQML aims to incorporate the symmetry inherent to the dataset with the QNN architecture so that the final prediction is *invariant* after the action of the symmetry group element on the original input feature.

Let us formalize it in a more concrete way. Consider a symmetry group \mathfrak{G} that acts on the data space \mathcal{X} . We say the training model is \mathfrak{G} -invariant if :

$$y_\theta(g[\mathbf{x}]) = y_\theta(\mathbf{x}), \forall \mathbf{x} \in \mathcal{X}, \forall g \in \mathfrak{G}. \quad (2)$$

In order to construct \mathfrak{G} -invariant model, we require three components: equivariant data embedding, equivariant QNN and invariant measurement [14].

First of all, we say that the data embedding is \mathfrak{G} -equivariant if the symmetry group element $g \in \mathfrak{G}$ applied on the data $\mathbf{x} \in \mathcal{R}$ induces a unitary quantum action $V_s[g]$ in the level of quantum states :

$$|\psi(g[\mathbf{x}])\rangle = V_s[g] |\psi(\mathbf{x})\rangle. \quad (3)$$

We call V_s the *induced representation* of the embedding $\psi(\mathbf{x})$ [14].

We also need to construct a trainable quantum circuit ansatz, parameterized by angles θ , which is equivariant with respect to the symmetry group \mathfrak{G} . For simplicity, we consider only the gates generated by a fixed generator $G \in \mathcal{G}$:

$$R_G(\theta) = \exp(-i\theta G), \theta \in \mathbb{R}. \quad (4)$$

where \mathcal{G} is a fixed gateset. For a symmetry group \mathfrak{G} and its representation V_s , the operator R_G is said to be \mathfrak{G} -equivariant if and only if [14], [17]:

$$[R_G(\theta), V_s[g]] = 0, \forall g \in \mathfrak{G}, \forall \theta \in \mathbb{R} \quad (5)$$

or equivalently,

$$[G, V_s[g]] = 0, \forall g \in \mathfrak{G}. \quad (6)$$

The definition of *equivariance* can also be extended to QNNs. We call that a QNN, \mathcal{U}_θ , is \mathfrak{G} -equivariant if and only if it consists of equivariant quantum operators, i.e. \mathcal{U}_θ commutes with all the components in the symmetric group \mathfrak{G} .

There exist several methods to construct the equivariant gateset [19], but in this paper, we will focus on the *twirling method*, which is the most practical approach for small symmetry groups [32]. Consider an arbitrary generator X . Then, we define a twirled operator $\mathcal{T}_\mathfrak{G}$ as :

$$\mathcal{T}_\mathfrak{G}[X] = \frac{1}{|\mathfrak{G}|} \sum_{g \in \mathfrak{G}} V_s[g]^\dagger X V_s[g]. \quad (7)$$

It corresponds to a projector of the operator X onto all symmetry group elements, commuting with $V_s[g]$ for all $g \in \mathfrak{G}$.

Finally, an observable O is \mathfrak{G} -invariant, if :

$$V_s[g]^\dagger O V_s[g] = O, \forall g \in \mathfrak{G}, \quad (8)$$

i.e. if O commutes with $V_s[g]$ for all $g \in \mathfrak{G}$. By taking all three components, the equivariance of QNN leads to the invariance of the final prediction:

$$\begin{aligned} y(g[\mathbf{x}]) &= \langle \psi(g[\mathbf{x}]) | \mathcal{U}(\theta)^\dagger O \mathcal{U}(\theta) | \psi(g[\mathbf{x}]) \rangle \\ &= \langle \psi(\mathbf{x}) | V_s^\dagger(\theta) \mathcal{U}(\theta)^\dagger O \mathcal{U}(\theta) V_s | \psi(\mathbf{x}) \rangle \\ &= \langle \psi(\mathbf{x}) | \mathcal{U}(\theta)^\dagger O \mathcal{U}(\theta) | \psi(\mathbf{x}) \rangle = y(\mathbf{x}) \end{aligned} \quad (9)$$

Overall, we have a trade-off between the equivariance and the expressibility of the QNN by constraining the quantum operators in the model based on the geometric prior of the dataset. GQML reduces the search space for training and brings advantages in many folds, such as trainability [18], convergence rate [33], and generalization power [14], [18].

III. GQML FOR IMAGE CLASSIFICATION

In this section, we will introduce Equivariant Quantum Convolutional Neural Networks (EquivQCNNs) for image classification invariant under the $p4m$ wallpaper symmetry group, \mathfrak{G}_{p4m} , which corresponds to the planar square symmetry group. It consists of 8 components :

- the identity e ,
- the rotation r , r^2 and r^3 of 90° , 180° , 270° around the origin,
- the reflection t_x and t_y in the x and y axis,
- the reflection in the two diagonals.

In this paper, we will focus on six components out of them, the rotation r and the reflection in the main axis, t_x and t_y .

A. Equivariant Data embedding

We will start by constructing the data embedding method for the reflectional and rotational symmetry of images. Amplitude encoding is one of the most fundamental methods for mapping classical data into quantum states [34]. In general, each pixel coordinate is associated with a computational basis by visualizing the 2D image as a 1D vector, but this complicates the manipulation of 2D symmetry.

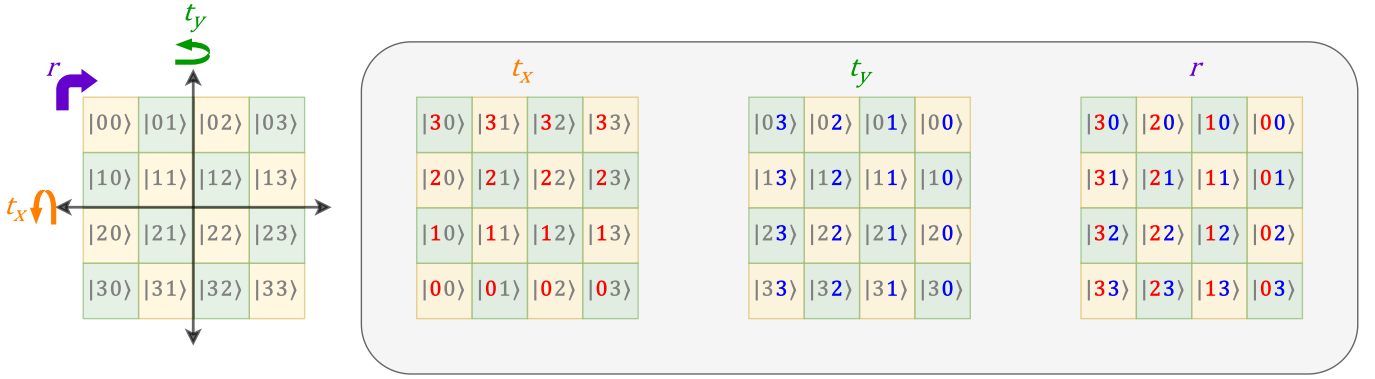


Fig. 1: Schematic diagram of the action of $p4m$ symmetry on 2D images of size 4×4 encoded using CAA embedding method with 2 qubits. The pixel at position (i, j) is associated with a computational basis $|i\rangle|j\rangle$.

We propose a *coordinate-aware* amplitude (CAA) embedding method, which facilitates finding the unitary representation of $p4m$ symmetry group. The main idea of the CAA embedding is that we can explicitly denote the x and y coordinates by using the first n qubits to represent the x -coordinate and the second n qubits for the y -coordinate of the pixel.

Let us consider a training set \mathcal{X} of 2-dimensional images with $N \times N$ pixels, denoted as $\mathbf{x} = \{x_{ij}\}$ with $i, j = 0, \dots, N-1$, each of which is associated with a hot encoded label $\ell \in \{0, 1\} \in \mathcal{Y}$. The CAA embedding maps the input image \mathbf{x} into a quantum state $|\psi(x)\rangle \in \mathcal{H}$ as follows:

$$|\psi(x)\rangle = \sum_{i=0}^{N-1} \sum_{j=0}^{N-1} x_{ij} |i\rangle|j\rangle \quad (10)$$

where $N = 2^n$. For simplicity, let us denote $q_{1:n}$ the first n -qubits for x -coordinates and $q_{n+1:2n}$ the second n -qubits for y -coordinates.

From the CAA embedding formulation, it is straightforward to find the induced representation of $p4m$ group elements. Fig. 1 visualizes CAA embedding of 2D images and the action of the symmetry elements on the computational basis states. Let us denote V_x and V_y the induced representation of the reflections, t_x and t_y respectively, and V_r for rotation of 90° , r , which are defined as follows :

$$V_x = X^{\otimes n} \otimes \mathbb{I}^{\otimes n} = X_{1:n}, \quad (11)$$

$$V_y = \mathbb{I}^{\otimes n} \otimes X^{\otimes n} = X_{n+1:2n}, \quad (12)$$

$$V_r = (X^{\otimes n} \otimes \mathbb{I}^{\otimes n}) \otimes_{i=0}^{n-1} SWAP_{i,i+n} = V_x V_r', \quad (13)$$

with $V_r' = \otimes_{i=0}^{n-1} SWAP_{i,i+n}$. Therefore, the quantum gates, which are equivariant with respect to $p4m$ symmetry, should commute with all the induced representation, $V_{p4m} = \{V_x, V_y, V_r\}$:

$$\begin{aligned} U \in \text{comm}\{V_x, V_y, V_r\} &= \text{comm}\{V_x, V_y, V_r'\} \\ &= \text{comm}\{X_{1:n}, X_{n+1:2n}, \otimes_{i=0}^{n-1} SWAP_{i,i+n}\}, \end{aligned} \quad (14)$$

where comm denotes the commutator of the unitary operators.

B. Equivariant Quantum Convolutional Neural Networks

First proposed by Iris Cong, *et al.* [35], Quantum Convolutional Neural Networks (QCNNs) is the quantum analogue of classical Convolutional Neural Networks (CNNs). QCNNs have exhibited success in different tasks, including quantum many-body problems [35], phase detection [8], and image classification [36], taking advantage of avoiding the barren plateaus with shallow circuit depth [11].

QCNN consists of two components, *convolutional filters*, which are k -body local quantum gates for $k < n$, and the pooling layers, to reduce the two qubit states into one qubit state. In most of the cases, we have $k = 2$ for convolutional filters, but in this paper, we will also introduce the case with $k > 2$ to maintain the equivariance. Especially QCNN maintains the translational invariance of input data by sharing identical parameters between the filters inside each layer.

Following the definition of equivariance and the method presented in Section II, we construct the equivariant ansatz of the convolutional filters for \mathfrak{G}_{p4m} . To start with, we can easily find out that the architecture of QCNN respects the equivariance with respect to V_r' as we repeat the same gate with the same parameter on qubit i and $i+n$ if we have an even n .

The ansatz symmetrization for the other symmetries requires more insights. We will consider the generator gateset, which only consists of Pauli strings up to 2-body local operation :

$$G = \{X, Y, Z, Y_1 Y_2, Z_1 Z_2\}. \quad (15)$$

For a single qubit gate, it is trivial to notice that only Pauli X gates commute with V_x, V_y , while for k -qubit gates for $k > 1$, we need to explore two cases separately.

1) G constrained to $q_{1:n}$ OR $q_{n+1:2n}$

Considering only 2-body quantum gates, finding $U \in \text{comm}(X_{1:n}, X_{n+1:2n})$ can be simplified into finding $U \in \text{comm}(X_1 X_2)$. We can easily find out that both $Y_1 Y_2$ and $Z_1 Z_2$ commute with $X_1 X_2$ applied on two qubits.

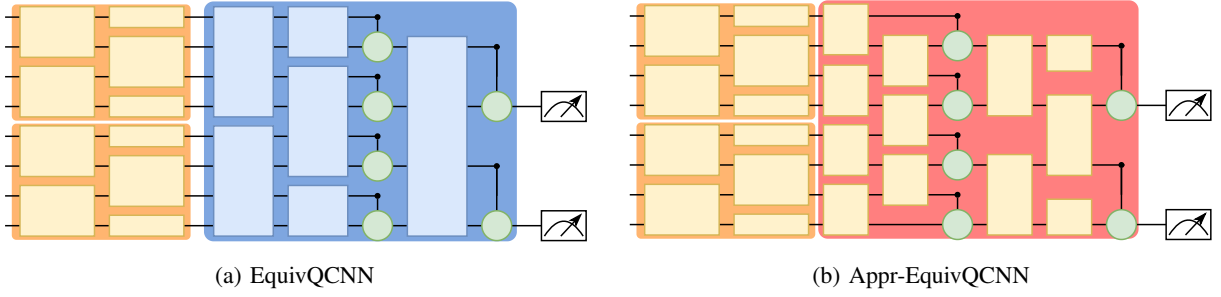


Fig. 2: A Schematic diagram of (a) EquivQCNN and (b) Appr-EquivQCNN for an example of 8 qubits to classify image of size 16×16 . They consist of U_2 (yellow rectangle) and U_4 (blue rectangle) convolutional filters (c.f. Fig. 3), followed by pooling layers (green circle). Both models contain a preliminary *scanning* phase, where U_2 acts on $q_{1:n}$ and $q_{n+1:2n}$ separately. EquivQCNN then consists of U_4 ansatz, while Appr-EquivQCNN is subject to a small noise by connecting $q_{1:n}$ and $q_{n+1:2n}$ with U_2 gate.

Indeed, using the Twirling method, we have :

$$\begin{aligned}
 \mathcal{T}_{X_1 X_2}(Y_1 Y_2) &= \frac{1}{2} \left(Y_1 Y_2 + (X_1 X_2)^\dagger (Y_1 Y_2) (X_1 X_2) \right) \\
 &= \frac{1}{2} (Y_1 Y_2 + X_1 Y_1 X_1 X_2 Y_2 X_2) \\
 &= \frac{1}{2} (Y_1 Y_2 + (-Y_1)(-Y_2)). \\
 &= Y_1 Y_2.
 \end{aligned} \tag{16}$$

Similarly, we can show that $Z_1 Z_2$ is the equivariant operator with respect to $X_1 X_2$. Thus, we obtain the equivariant generator gateset :

$$G_{s,1} = \{Y_1 Y_2, Z_1 Z_2\}. \tag{17}$$

2) **G applied on both $q_{1:n}$ AND $q_{n+1:2n}$**

Unlike the first case, where the Pauli X gate in V_x and V_y acts equally on two qubits with $X \otimes X$, the weight of Pauli gates is unbiased in this case. We can easily notice that $G_{s,1}$ acting on q_n and q_{n+1} do not commute with V_x and V_y , as :

$$[X_1 \otimes \mathbb{I}_2, Y_1 Y_2] = -[Y_1 Y_2, X_1 \otimes \mathbb{I}_2]. \tag{18}$$

Indeed, in order to construct an equivariant operator, we need an even number of Pauli Y or Pauli Z gates applied on both $q_{1:n}$ and $q_{n+1:2n}$ [19]. Therefore, the smallest equivariant quantum gates are :

$$G_{s,2} = \{P_\sigma P_\sigma P_{\sigma'} P_{\sigma'} | P_{\sigma, \sigma'} \in \{X, Y, Z\}\} \tag{19}$$

By exponentiating the equivariant generators found above, we can construct the convolutional filter ansatz, which is equivariant with respect to V_{p4m} . Fig. 3 summarizes the equivariant two-qubit convolutional filter ansatz, U_2 and the four-qubit ansatz, U_4 . Using the U_2 and U_4 , we propose two QCNN models, Equivariant QCNN (EquivQCNN) and Approximately Equivariant QCNN (Appr-EquivQCNN), as shown in Fig. 2. In both cases, we first apply the two-qubit convolutional filters on $q_{1:n}$, and $q_{n+1:2n}$ separately, without connecting them, which can be considered as the preliminary scanning phase. Then, in EquivQCNN, U_4 ansatz is used as the convolutional filter

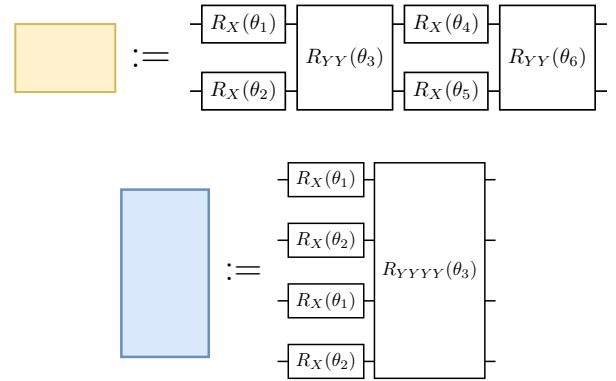


Fig. 3: Parameterized quantum circuits ansatz, U_2 (yellow rectangle) and U_4 (blue rectangle), used the convolutional filters equivariant with respect to $p4m$ symmetry group.

and connects $q_{1:n}$, and $q_{n+1:2n}$, leading the fully equivariant model. On the other hand, in Appr-EquivQCNN, U_2 ansatz is repeated for the learning layers acting on q_n , and q_{n+1} . We add a limited noise to the equivariant model to increase the expressibility by slightly breaking the symmetry. With this noise, we aim to find a crossing point between the expressibility and the equivariance so that it is expressible enough to learn the training samples but, at the same time, not excessively expressible to generalize.

C. *Approximately Invariant Measurement*

In this section, we propose an *Approximately Invariant Measurement*, with the detailed process summarized in Fig. 4. For simplicity, we will consider the binary classification case.

Let us call $q_{i_m} \in q_{1:n}$ and $q_{i_m+n} \in q_{n+1:2n}$ with $i_m \in [1, \dots, n]$ the qubits which are not traced out in EquivQCNN and measured at the end of the circuit. First, we apply an $R_z(\phi)$ and a Hadamard gate on both q_{i_m} and q_{i_m+n} , with ϕ also a trained parameter. Then, we measure the probability distribution of state $|0\rangle$ and $|1\rangle$ on each of the qubits separately, obtaining $[p_0, p_1]$ and $[p'_0, p'_1]$ respectively. As the other qubits are traced out, only the two-qubit state is left at the end of

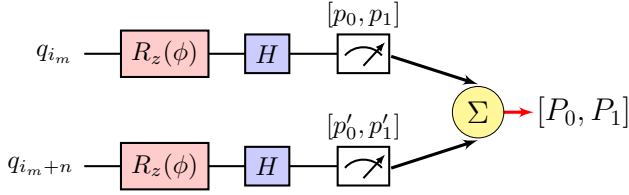


Fig. 4: Approximately Invariant Measurement process. We apply $R_z(\phi)$ and H gate on two qubits, $q_{i_m} \in q_{1:n}$ and $q_{i_m+n} \in q_{n+1:2n}$, and measure the probability distribution on each qubits separately. The final label is computed by summing up the two distributions and taking its half.

the quantum circuit. Denoting the final quantum state on the qubit q_{i_m} and q_{i_m+n} as $|\psi_f\rangle = r_0 e^{i\theta_0} |00\rangle + r_1 e^{i\theta_1} |01\rangle + r_2 e^{i\theta_2} |10\rangle + r_3 e^{i\theta_3} |11\rangle$, the proposed measurement on q_{i_m} returns the probability distribution :

$$p_0 = \frac{1}{2} [r_0^2 + r_1^2 + 2r_0 r_1 \cos(2\phi - \theta_0 + \theta_1) + r_2^2 + r_3^2 + 2r_2 r_3 \cos(2\phi - \theta_2 + \theta_3)], \quad (20)$$

$$p_1 = \frac{1}{2} [r_0^2 + r_1^2 - 2r_0 r_1 \cos(2\phi - \theta_0 + \theta_1) + r_2^2 + r_3^2 - 2r_2 r_3 \cos(2\phi - \theta_2 + \theta_3)]. \quad (21)$$

First of all, we can easily notice that the measurement is invariant with respect to V_r' as we are summing up the final measurement on q_{i_m} and q_{i_m+n} . Now, let us prove that it is equivariant with a certain error rate ϵ . Similarly, let us call $[p_0^x, p_1^x]$ the final probability of the image reflected with respect to the x -axis for the final state $V_x |\psi_f\rangle = r_1 e^{i\theta_1} |00\rangle + r_0 e^{i\theta_0} |01\rangle + r_3 e^{i\theta_3} |10\rangle + r_2 e^{i\theta_2} |11\rangle$ with a bit flip on qubit q_{i_m} . By performing the same computation, we can compute the difference between p_0 and p_0^x :

$$\begin{aligned} p_0 - p_0^x &= r_0 r_1 [\cos(2\phi - \theta_0 + \theta_1) - \cos(2\phi + \theta_0 - \theta_1)] \\ &\quad + r_2 r_3 [\cos(2\phi - \theta_2 + \theta_3) - \cos(2\phi + \theta_2 - \theta_3)] \\ &= \sin(2\phi) [r_0 r_1 \sin(\theta_1 - \theta_0) + r_2 r_3 \sin(\theta_3 - \theta_2)] \\ &\leq \frac{1}{2} \epsilon [\sin(\theta_2 - \theta_1) + \sin(\theta_3 - \theta_2)], \end{aligned} \quad (22)$$

with $\epsilon = \sin(2\phi)$. The last inequality uses $\max r_0 r_1 + r_2 r_3 = \frac{1}{2}$ while taking into account the fact that $r_0^2 + r_1^2 + r_2^2 + r_3^2 = 1$. This proves that with $\phi \approx 0$ or $\phi \approx \frac{\pi}{2}$, we can say that the measurement is *approximately invariant* with respect to V_x , and also V_y by using the same justification. The presence of the R_z gate loosens the constraint imposed by the symmetry and adds an extra degree of freedom to the training. By trading off the *full* invariance and expressibility, we allow exploring larger search space for better performance.

We can generalize this measurement for L -class classification by measuring $\log_2 L$ qubits at $q_{1:n}$ and $q_{n+1:2n}$ qubits separately and summing them up. This way of measurement corresponds to the *Softmax* activation function at the end of

the neural network. Thus, we use the binary cross entropy to calculate the training loss,

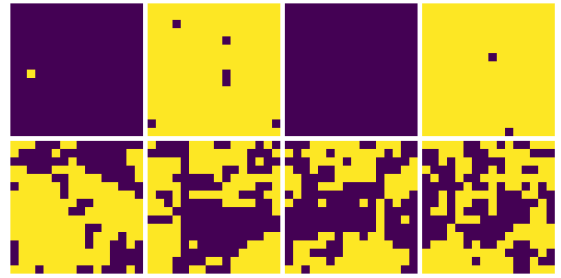
$$\mathcal{L}_\theta(\mathbf{x}) = - \sum_{i=1}^L \ell_i \log p_i(\theta; \mathbf{x}), \quad (23)$$

where $\ell = [\ell_1, \ell_2, \dots, \ell_L]$ with $\ell_i \in \{0, 1\}$ is the one-hot encoded target label. The state with the highest probability will correspond to the class with which the input image is associated.

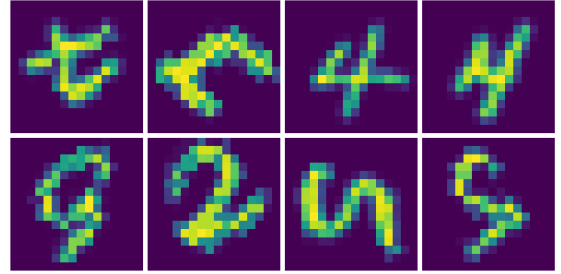
For the following, we will consider two different types of measurements :

- 1) M_1 : ϕ is constrained to zero, $\phi = 0$,
- 2) M_2 : ϕ is updated during the training, $\phi \neq 0$.

IV. RESULT



(a) Ising model



(b) Extended MNIST

Fig. 5: Examples of the Ising model and the extended MNIST image samples with size 16×16 used for binary classification. Each row corresponds to each class.

In this section, we present our preliminary results of the EquivQCNN training for binary image classification applied to two different image datasets, shown on Fig. 5. The first dataset contains the spin distribution of the 2D lattice Ising model with 16×16 interacting spins, simulated using Metropolis Monte Carlo with the Hamiltonian [37]:

$$H = -J \sum_{\langle ij \rangle} s_i s_j, \quad (24)$$

where $s_i \in \{-1, 1\}$ corresponds to the spin on site i , J the interaction between two spins and $\langle ij \rangle$ the pairs of the nearest neighbours. At low temperature T , the spins are ordered, pointing all in the same direction, and as the temperature increases, we reach the critical temperature T_c where we observe the phase transition from an ordered phase to a

disordered phase. By taking the periodic boundary condition, the Ising model dataset is reflectional and rotational symmetric by construction. We aim to classify the order phase from the disordered phase using EquivQCNN.

The second dataset is the extended MNIST dataset, which also includes randomly reflected and rotated handwritten digit images. In this paper, we present the results for the classification of digits 4 and 5, downsampled into 16×16 pixels.

We compare the performance of EquivQCNN with a non-equivariant QCNN with a similar number of parameters, using a convolutional filter that generates an arbitrary two-qubit SO_4 state [36]. For all the models, the initial parameters are sampled randomly from a uniform distribution, $[-0.1, 0.1]$. The parameters are updated with ADAM optimizers, using the learning rate of 0.01, $\beta_1 = 0.5$ and $\beta_2 = 0.999$.

$n_{samples}$	Ising		MNIST	
	40	10240	40	10240
Non-Equiv.	77.6 ± 0.1	83.0 ± 2.0	66.7 ± 2.1	72.9 ± 0.5
Equiv.	74.2 ± 0.2	75.8 ± 0.3	77.5 ± 1.0	74.5 ± 4.7
Appr-Eq. 1	84.8 ± 2.2	85.4 ± 2.0	52.9 ± 0.1	72.7 ± 2.4
Appr-Eq. 2	86.4 ± 3.4	89.3 ± 2.9	69.7 ± 2.9	76.2 ± 1.8

TABLE I: The test accuracy at the end of the QCNN training for Ising and extended MNIST with $n_{samples} = 40$ and 10240 training samples (best result in bold).

To prove the generalization power of the EquivQCNN, we train the models for different training set size, $N_s = 2^i \cdot 10$ for $i = 1, \dots, 10$ with the batch size $N_{bs} = 2^i$ to maintain the same number of updates in each epoch. Tab. I and Fig. 6 summarize the test accuracy obtained at the end of the training with different QCNN architectures. Note that the number of samples in the test set is always the same regardless of the number of training samples.

We can observe that EquivQCNN and Appr-EquivQCNN with M_2 measurement have higher test accuracy for all N_s , especially for small N_s . In particular, in the case of the Ising model, Appr-EquivQCNN with M_2 outperforms the non-equivariant model only using 256 times less number of training samples. This certainly proves that the equivariance helps to improve the generalization power as expected.

One interesting point is that EquivQCNN gives the best result for MNIST, while Appr-EquivQCNN with M_2 measurement outperforms EquivQCNN for the Ising model. This difference might be explained by the fact that the Ising model is subject to a stricter symmetry by its construction, compared to the extended MNIST, where the symmetry is artificially created by random reflection and rotation. Thus, injecting noise into the model with Appr-EquivQCNN helps training for the Ising dataset, which is not the case for MNIST.

V. CONCLUSION

In this paper, we introduced the Equivariant QCNN for the planar wallpaper symmetry group $p4m$, including reflection and 90° rotation in image classification. Furthermore, our study suggests the possibility of injection of noises into the GQML model in order to find the best crossing point

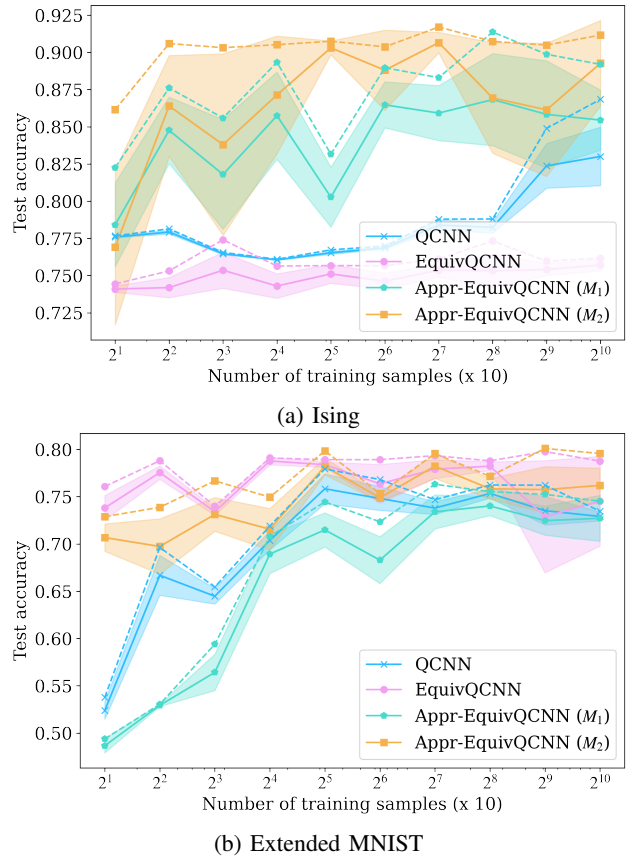


Fig. 6: The test accuracy obtained at the end of QCNN training for Ising and extended MNIST dataset with different training sample numbers. The solid line corresponds to the average over the five runs, and the dashed line the best one among them. The test accuracy for EquivQCNN and ApprEquivQCNN with M_2 are always higher than the non-equivariant QCNN, proving their generalization power.

between expressibility and equivariance. The proposed models are tested for two different datasets, the Ising model and the extended MNIST dataset, and compared with the non-equivariant model. The results obtained clearly proved that the EquivQCNN outperforms the non-equivariant one in terms of generalization power, especially with a small training set size. Previous studies on QML have already proven that it has a high generalization power with a small training set size [7]. This work demonstrated that we can further improve the generalization thanks to the induced bias added by the geometric prior to the dataset.

For our future research, we plan to compare the EquivQCNN with the problem-agnostic model, not only in terms of test accuracy but also in other factors, such as local effective dimension, overparameterization, barren plateaus, etc. Ultimately, we extend the test to a more realistic use case with a larger image size where symmetry is an essential component for the training, such as Earth Observation images, and show the practical advantage of EquivQCNN.

ACKNOWLEDGEMENT

This work was carried out as part of the quantum computing for earth observation (QC4EO) initiative of ESA Φ -lab, partially funded under contract 4000135723/21/I-DT-Ir, in the FutureEO programme. MG and SF are supported by CERN through the CERN QTI.

REFERENCES

- [1] Maria Schuld and Francesco Petruccione. *Machine Learning with Quantum Computers*. Springer International Publishing, 2021.
- [2] Vojtěch Havlíček, Antonio D. Córcoles, Kristan Temme, Aram W. Harrow, Abhinav Kandala, Jerry M. Chow, and Jay M. Gambetta. Supervised learning with quantum-enhanced feature spaces. *Nature*, 567(7747):209–212, Mar 2019.
- [3] M. Cerezo, Andrew Arrasmith, Ryan Babbush, Simon C. Benjamin, Suguru Endo, Keisuke Fujii, Jarrod R. McClean, Kosuke Mitarai, Xiao Yuan, Lukasz Cincio, and Patrick J. Coles. Variational quantum algorithms. *Nature Reviews Physics*, 3(9):625–644, Aug 2021.
- [4] Hsin-Yuan Huang, Michael Broughton, Masoud Mohseni, Ryan Babbush, Sergio Boixo, Hartmut Neven, and Jarrod R. McClean. Power of data in quantum machine learning. *Nature Communications*, 12(1):2631, May 2021.
- [5] Yunchao Liu, Srinivasan Arunachalam, and Kristan Temme. A rigorous and robust quantum speed-up in supervised machine learning. *Nature Physics*, 17(9):1013–1017, Sep 2021.
- [6] Seth Lloyd, Masoud Mohseni, and Patrick Rebentrost. Quantum algorithms for supervised and unsupervised machine learning. arXiv:1307.0411, 2013.
- [7] Matthias C. Caro, Hsin-Yuan Huang, M. Cerezo, Kunal Sharma, Andrew Sornborger, Lukasz Cincio, and Patrick J. Coles. Generalization in quantum machine learning from few training data. *Nature Communications*, 13(1):4919, Aug 2022.
- [8] Saverio Monaco, Oriel Kiss, Antonio Mandarino, Sofia Vallecorsa, and Michele Grossi. Quantum phase detection generalization from marginal quantum neural network models. *Phys. Rev. B*, 107:L081105, Feb 2023.
- [9] Michał Siemaszko, Adam Buraczewski, Bertrand Le Saux, and Magdalena Stobińska. Rapid training of quantum recurrent neural networks. *Quantum Machine Intelligence*, 5(2):31, Jul 2023.
- [10] Zoë Holmes, Kunal Sharma, M. Cerezo, and Patrick J. Coles. Connecting ansatz expressibility to gradient magnitudes and barren plateaus. *PRX Quantum*, 3(1), Jan 2022.
- [11] Arthur Pesah, M. Cerezo, Samson Wang, Tyler Volkoff, Andrew T. Sornborger, and Patrick J. Coles. Absence of barren plateaus in quantum convolutional neural networks. *Physical Review X*, 11(4), Oct 2021.
- [12] M. Cerezo, Akira Sone, Tyler Volkoff, Lukasz Cincio, and Patrick J. Coles. Cost function dependent barren plateaus in shallow parametrized quantum circuits. *Nature Communications*, 12(1), Mar 2021.
- [13] Sujay Kazi, Martin Larocca, and M. Cerezo. On the universality of s_n -equivariant k -body gates. arXiv:2303.00728, 2023.
- [14] Johannes Jakob Meyer, Marian Mularski, Elies Gil-Fuster, Antonio Anna Mele, Francesco Arzani, Alissa Wilms, and Jens Eisert. Exploiting symmetry in variational quantum machine learning. *PRX Quantum*, 4:010328, Mar 2023.
- [15] Han Zheng, Gokul Subramanian Ravi, Hanrui Wang, Kanav Setia, Frederic T. Chong, and Junyu Liu. Benchmarking variational quantum circuits with permutation symmetry. arXiv:2211.12711, 2022.
- [16] Michael Ragone, Paolo Braccia, Quynh T. Nguyen, Louis Schatzki, Patrick J. Coles, Frederic Sauvage, Martin Larocca, and M. Cerezo. Representation theory for geometric quantum machine learning. arXiv:2210.07980, 2023.
- [17] Martín Larocca, Frédéric Sauvage, Faris M. Sباهي, Guillaume Verdon, Patrick J. Coles, and M. Cerezo. Group-invariant quantum machine learning. *PRX Quantum*, 3(3), Sep 2022.
- [18] Louis Schatzki, Martin Larocca, Quynh T. Nguyen, Frederic Sauvage, and M. Cerezo. Theoretical guarantees for permutation-equivariant quantum neural networks. arXiv:2210.09974, 2022.
- [19] Quynh T. Nguyen, Louis Schatzki, Paolo Braccia, Michael Ragone, Patrick J. Coles, Frederic Sauvage, Martin Larocca, and M. Cerezo. Theory for equivariant quantum neural networks. arXiv:2210.08566, 2022.
- [20] Michael M. Bronstein, Joan Bruna, Taco Cohen, and Petar Veličković. Geometric deep learning: Grids, groups, graphs, geodesics, and gauges. arXiv:2104.13478, 2021.
- [21] Taco S. Cohen and Max Welling. Group equivariant convolutional networks. arXiv:1602.07576, 2016.
- [22] Simon Batzner, Albert Musaelian, Lixin Sun, Mario Geiger, Jonathan P. Mailoa, Mordechai Kornbluth, Nicola Molinari, Tess E. Smidt, and Boris Kozinsky. E(3)-equivariant graph neural networks for data-efficient and accurate interatomic potentials. *Nature Communications*, 13(1), May 2022.
- [23] Jonas Kübler, Simon Buchholz, and Bernhard Schölkopf. The inductive bias of quantum kernels. In M. Ranzato, A. Beygelzimer, Y. Dauphin, P.S. Liang, and J. Wortman Vaughan, editors, *Advances in Neural Information Processing Systems*, volume 34, pages 12661–12673. Curran Associates, Inc., 2021.
- [24] Maxwell West, Martin Sevier, and Muhammad Usman. Reflection equivariant quantum neural networks for enhanced image classification. arXiv:2212.00264, 2023.
- [25] Nishant Dave, Vivek Vinze, Jainam Dhama, Neha Katre, and Stevina Correia. Study of group equivariant convolutional networks for image classification. In *2021 International Conference on Advances in Computing, Communication, and Control (ICAC3)*, pages 1–5, 2021.
- [26] Diego Marcos, Michele Volpi, Nikos Komodakis, and Devis Tuia. Rotation equivariant vector field networks. In *Proceedings of the IEEE International Conference on Computer Vision (ICCV)*, Oct 2017.
- [27] Mercedes E. Paoletti, Juan M. Haut, Swalpa Kumar Roy, and Eligius M. T. Hendrix. Rotation equivariant convolutional neural networks for hyperspectral image classification. *IEEE Access*, 8:179575–179591, 2020.
- [28] Alessandro Sebastianelli, Daniela Alessandra Zaidenberg, Dario Spiller, Bertrand Le Saux, and Silvia Liberata Ullo. On circuit-based hybrid quantum neural networks for remote sensing imagery classification. *IEEE Journal of Selected Topics in Applied Earth Observations and Remote Sensing*, 15:565–580, 2022.
- [29] Su Yeon Chang, Bertrand Le Saux, Sofia Vallecorsa, and Michele Grossi. Quantum convolutional circuits for earth observation image classification. In *IGARSS 2022 - 2022 IEEE International Geoscience and Remote Sensing Symposium*, pages 4907–4910, 2022.
- [30] Yan Li, Guitao Cao, and Wenming Cao. A dynamic group equivariant convolutional networks for medical image analysis. In *2020 IEEE International Conference on Bioinformatics and Biomedicine (BIBM)*, pages 1056–1062, 2020.
- [31] Alexander Bogatskiy, Brandon Anderson, Jan T. Offermann, Marwah Roussi, David W. Miller, and Risi Kondor. Lorentz group equivariant neural network for particle physics. arXiv:2006.04780, 2020.
- [32] J. Helsen. *Quantum information in the real world: Diagnosing and correcting errors in practical quantum devices*. PhD thesis, 2019.
- [33] Han Zheng, Zimu Li, Junyu Liu, Sergii Strelchuk, and Risi Kondor. Speeding up learning quantum states through group equivariant convolutional quantum ansätze. *PRX Quantum*, 4:020327, May 2023.
- [34] Maria Schuld and Nathan Killoran. Quantum machine learning in feature hilbert spaces. *Phys. Rev. Lett.*, 122:040504, Feb 2019.
- [35] Iris Cong, Soonwon Choi, and Mikhail D. Lukin. Quantum convolutional neural networks. *Nature Physics*, 15(12):1273–1278, Aug 2019.
- [36] Tak Hur, Leeseok Kim, and Daniel K. Park. Quantum convolutional neural network for classical data classification. *Quantum Machine Intelligence*, 4(1), Feb 2022.
- [37] Lars Onsager. Crystal statistics. i. a two-dimensional model with an order-disorder transition. *Phys. Rev.*, 65:117–149, Feb 1944.